Atomistic Modeling of Intrinsically Disordered Proteins Under PEG Crowding: Quantitative Comparison with Experimental Data and Implication of Protein-Crowder Attraction

Valery Nguemaha,[†] Sanbo Qin,[†] and Huan-Xiang Zhou[*,†,‡]

[†]Department of Physics and Institute of Molecular Biophysics, Florida State University, Tallahassee, Florida 32306, United States

[‡]Department of Chemistry and Department of Physics, University of Illinois at Chicago, Chicago, Illinois 60607, United States

Supplementary Information

Table S1. Conformational properties of IDPs in the absence and presence of crowders.[a]

	0%			10%			20%		
IDP	b (Å^{-1})	mean R_g (Å)		$\bar{E}$			$\bar{E}$		
		raw	reweighted	Expt	st only	st + at	Expt	st only	st + at
IN	.0269	18.51	19.72	0.672	0.719	0.682	0.689	0.761	0.712
ACTR	.0161	20.90	21.91	0.523	0.594	0.547	0.560	0.683	0.613
ProTαN	.0882	24.74	28.52	0.398	0.423	0.385			
ProTαC	.1137	24.75	29.40	0.330	0.337	0.306			

[a]IDP conformations generated by TRaDES.

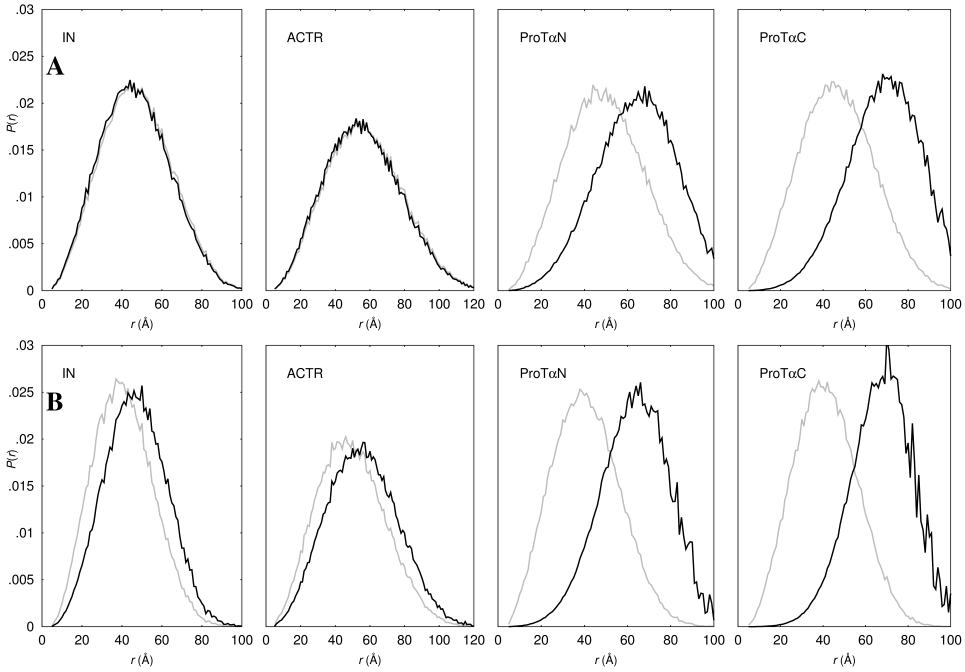

Figure S1. Distributions of the donor-acceptor distance *r*. (**A**) The raw *r* distributions generated for four IDP sequences by flexible-mecchano (gray curves) and those after the $\exp(br_n)$ reweighting to match experimental crowder-free FRET efficiencies (black curves). (**B**) Corresponding results for TRaDES.

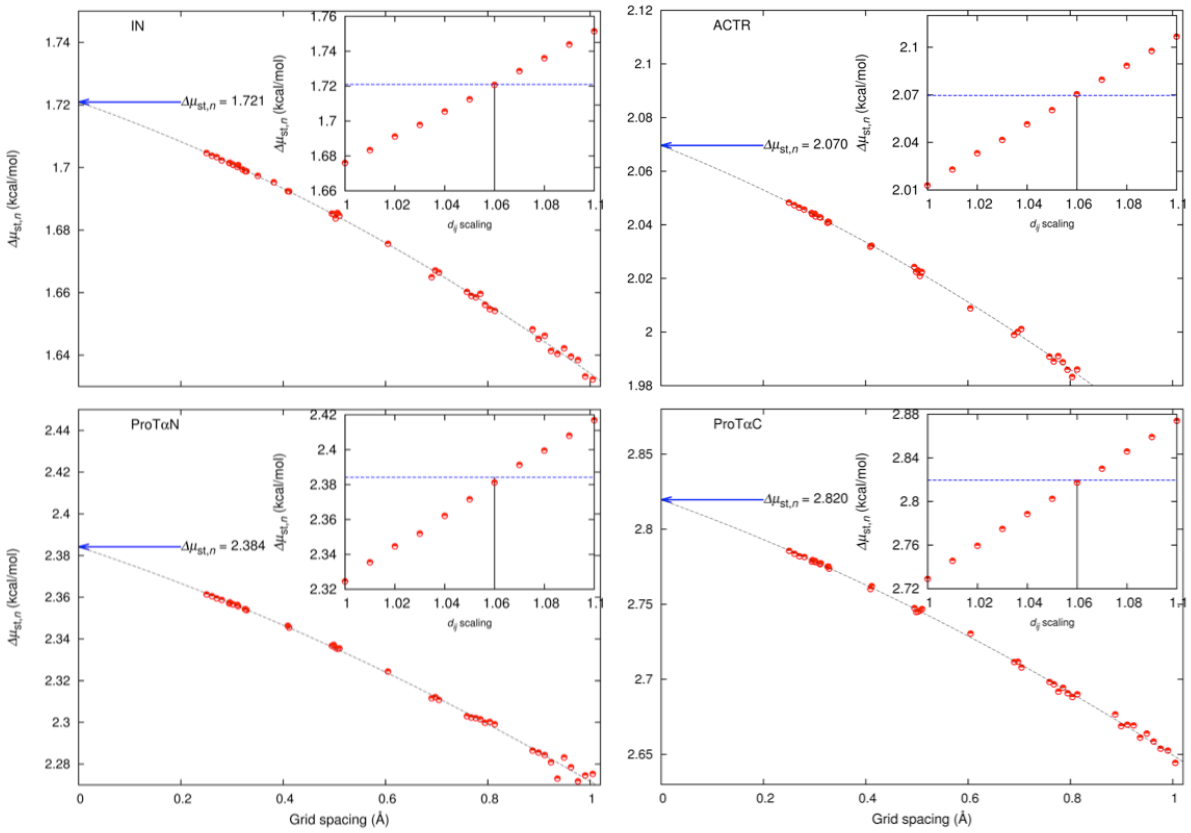

Figure S2. Correcting for numerical errors due to discretization in FMAP calculations. Using one conformation of an IDP and one PEG 6000 configuration at a 10% weight fraction, the chemical potential $\Delta\mu_{\mathrm{st},n}$ due to steric repulsion was calculated at a range of grid spacings for FFT discretization. The dependence of $\Delta\mu_{\mathrm{st},n}$ on grid spacing was then fitted to a parabolic function and extrapolated to zero grid spacing as the true value (indicated by a horizontal arrow). Note that the $\Delta\mu_{\mathrm{st},n}$ value at a finite grid spacing, e.g., 0.6 Å underestimated the true value. To compensate, $\Delta\mu_{\mathrm{st},n}$ values at a fixed grid spacing of 0.6 Å were calculated with the interatomic contact distances d_{ij} inflated at various amounts (*inset*). A 6% inflation in d_{ij} was able to reproduce the $\Delta\mu_{\mathrm{st},n}$ true values (horizontal dash in *inset*) for all the four IDPs.

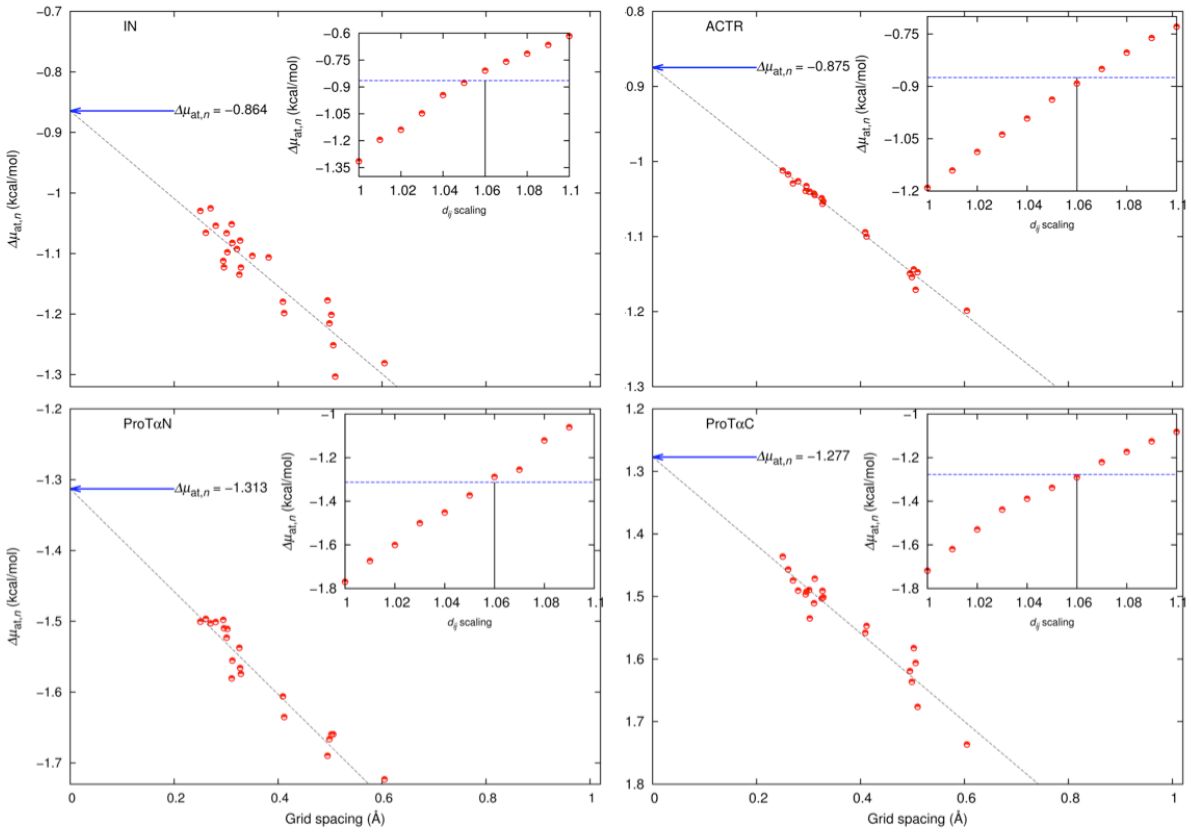

Figure S3. Correcting for numerical errors due to discretization in FMAP calculations. Similar to Fig. S2, but here the correction is for $\Delta\mu_{\mathrm{at},n}$. The same procedure was used, except that the dependence of $\Delta\mu_{\mathrm{at},n}$ on grid spacing was fitted to a linear function.

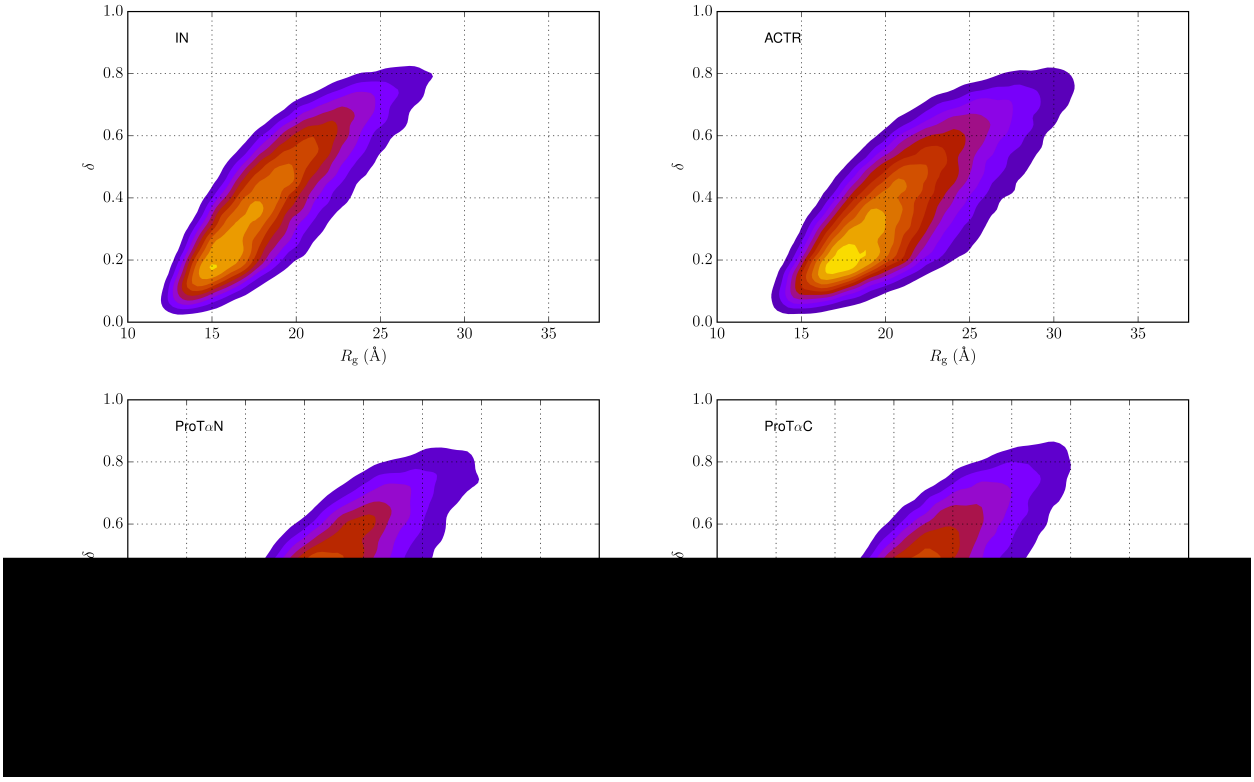

Figure S4. Two-dimensional probability densities in radius of gyration and asphericity for four IDPs, calculated from reweighted TRaDES conformational ensembles.

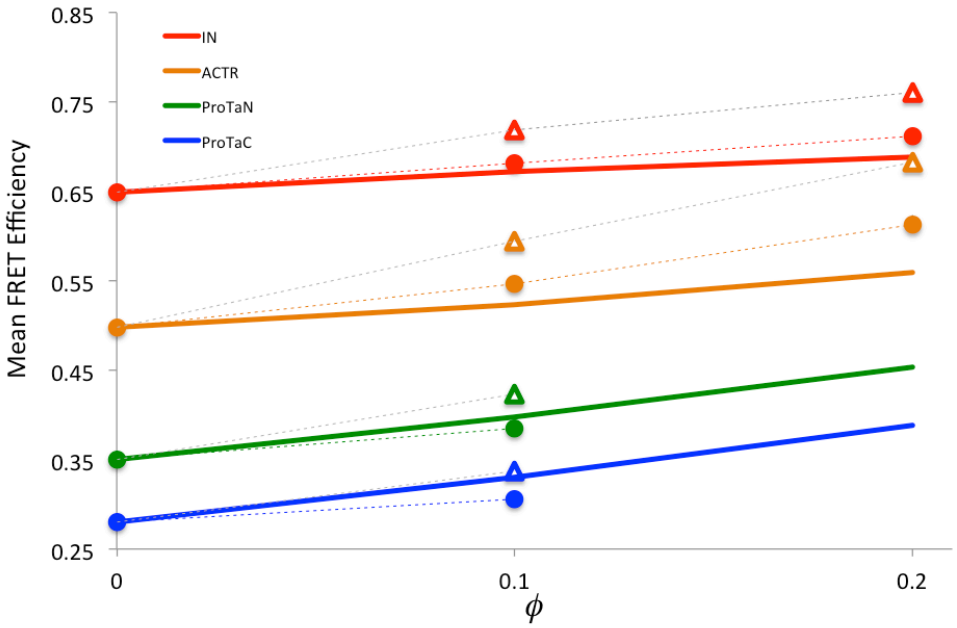

Figure S5. Experimental and calculated mean FRET efficiencies. Experimental results are shown as solid lines, calculated results are shown as triangles or circles (connected by dash), when only steric repulsion or both steric repulsion and weak attraction between IDPs and PEG are accounted for. Calculated results are from applying FMAP on reweighted TRaDES conformational ensembles; errors, as estimated by bootstrapping, are less than the size of the symbols.

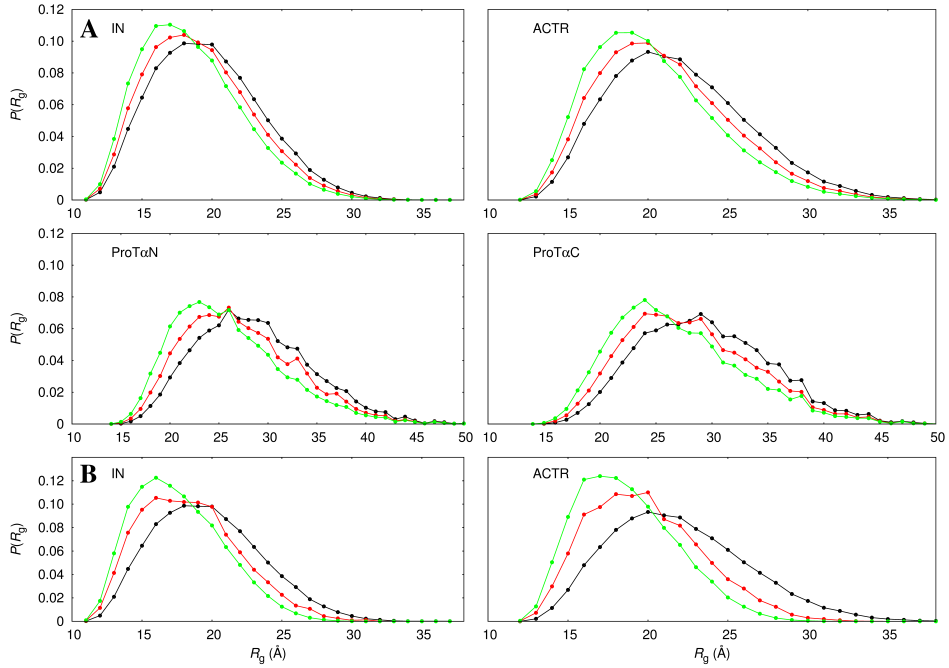

Figure S6. R_g distributions of the four proteins in the absence and presence of PEG 6000. (**A**) 10% PEG 6000. (**B**) 20% PEG 6000. Results calculated from reweighted TRaDES conformational ensembles are in black; those shifted by PEG modeled with steric repulsion only are in green; and those shifted by PEG modeled with both steric repulsion and weak attraction are in red.